UNIVERSITÀ DI PARMA

ARCHIVIO DELLA RICERCA

University of Parma Research Repository

Heterogenization of a [NiFe] Hydrogenase Mimic through Simple and Efficient Encapsulation into a Mesoporous MOF

note finali coverpage

(Article begins on next page)

06 February 2025

Inorganic Chemistry

Heterogenization of a [NiFe] Hydrogenase Mimic through Simple and Efficient Encapsulation into a Mesoporous MOF

Davide Balestri,[†] Yoann Roux,[‡] Monica Mattarozzi,[†] Claudio Mucchino,[†] Laurent Heux,[§] Deborah Brazzolotto,[‡,∥] Vincent Artero,[∥] Carole Duboc,[‡] Paolo Pelagatti,*[†,⊥] Luciano Marchio,*[†] and Marcello Gennari*[‡]

[†]Dipartimento di Scienze Chimiche, della Vita e della Sostenibilità Ambientale, Università degli Studi di Parma, Parco Area delle Scienze 17A, 43124 Parma, Italy

[‡]Département de Chimie Moléculaire (DCM), UMR 5250 Université Grenoble Alpes, CNRS, 38000 Grenoble, France

[§]Centre de Recherche sur les Macromolécules Végétales (CERMAV), UPR 5301, Université Grenoble Alpes, CNRS, 38000 Grenoble, France

[∥]Laboratoire Chimie et Biologie des Métaux (LCBM), UMR 5249 Université Grenoble Alpes, CNRS, 38000 Grenoble, France

[⊥]Centro Interuniveristario di Reattività Chimica e Catalisi (CIRCC), Via Celso Ulpiani 27, 70126 Bari, Italy

S *Supporting Information*

ABSTRACT: In the quest for new, efficient, and noble-metal-free H_2-evolution catalysts, hydrogenase enzymes are a source of inspiration. Here, we describe the development of a new hybrid material based on a structural and functional [NiFe]-hydrogenase model complex (**NiFe**) incorporated into the Zr-based MOF PCN-777. The bulk **NiFe@PCN-777** material was synthesized by simple encapsulation. Characterization by solid-state NMR and IR spectroscopy, SEM-EDX, ICP-OES, and gas adsorption confirmed the inclusion of the guest. FTO-supported thin films of the **NiFe@PCN-777** composite were obtained by electrophoretic deposition of the bulk material and characterized by SEM-EDX, ICP-OES, and cyclic voltammetry. The average surface concentration of electroactive **NiFe** catalyst in the film was found to be $\sim 9.6 \times 10^{-10}$ mol cm^{-2}, implying that a surprisingly high fraction (37%) of **NiFe** units incorporated in the MOF are electroactive. By cyclic voltammetry, we showed that **NiFe** maintains its electrocatalytic capabilities for H^+ reduction inside the MOF cavities, even if under controlled-potential electrolysis conditions the activity of **NiFe** cannot be discerned from that of free PCN-777 and FTO.
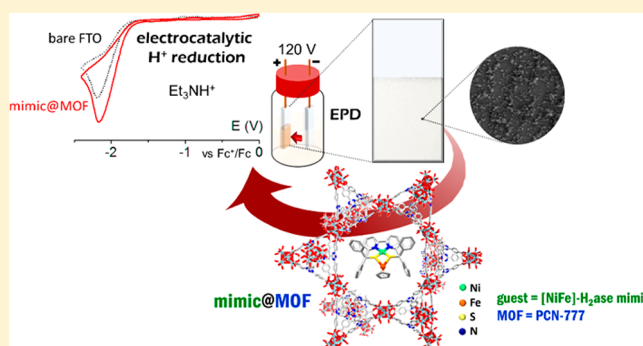
1. INTRODUCTION

In the current context of increasing global energy demand, hydrogen produced from catalytic water splitting is a promising, clean, and renewable fuel for the future.[1,2] Platinum is the state of the art catalyst for H_2 evolution from water, but its limited abundance in the earth's crust and high cost have stimulated the development of alternative noble-metal-free hydrogen evolution catalysts.[3,4] In nature, hydrogenase enzymes (H_2ases) catalyze proton reduction to H_2 at high rates and close to the thermodynamic equilibrium, exclusively employing inexpensive and abundant first-row transition metals (nickel and/or iron).[5,6] Hydrogenases thus represent an inspiration for the design of new molecular H_2-evolution catalysts. Both major classes of hydrogenases, the [FeFe]- and [NiFe]-H_2ases, feature a bis-thiolate-bridged dinuclear complex (FeFe or NiFe, respectively) at their active site.[5] Even though many efforts have been made toward the development of synthetic structural and functional mimics, most of the isolated complexes suffer from a limited stability under catalytic conditions.[7−10]

In the attempt to address these issues, one strategy relies on the confinement of reported H_2-evolution molecular catalysts[11−16] into the cavities of solid-state porous scaffolds, such as metal−organic frameworks (MOFs).[14,15,17−27] MOFs are crystalline, microporous, or nanoporous solids with exceptionally high surface area consisting of a periodic lattice built up from the assembly of small metal aggregates and organic linkers.[28−32] The incorporation of molecular catalysts in the uniformly distributed inner pores and channels of MOFs allows a high dispersion and isolation of the catalytic sites and a thorough control of their microenvironment: (i) the high site dispersion in the reticular structure of MOFs results in a high density of active centers in the material, thus enhancing the catalytic efficiency of the process;[33] (ii) the spatial isolation of the catalytic sites in the framework is expected to improve the stability of the molecular complexes, limiting catalyst

 A

65 deactivation or undesired intermolecular side reactions during
66 turnover; (iii) the chemical versatility of MOFs gives a unique
67 possibility to tailor the dimensionality and polarity of the
68 cavities, which can then act as the pockets of enzymes, inducing
69 second coordination sphere effects on the active guest and
70 stabilizing reaction intermediates.[12,34,35]

71 An increasing number of contributions have reported on the
72 incorporation of H_2-evolving catalysts (including molecular
73 complexes and inorganic nanoparticles) into MOFs. Interest-
74 ingly, in most cases an increase in their stability and/or
75 reactivity for electro- or photochemically driven proton
76 reduction has been observed.[14,15,17−25] However, to the best
77 of our knowledge only a few reports concern the insertion of
78 hydrogenase mimics into MOFs,[12] and all of them are based on
79 a photochemical approach involving a sacrificial electron donor.
80 In particular, the groups of Ott[22,26,27,36] and Feng[21] grafted
81 [FeFe]-hydrogenase mimics to zirconium (or, more recently,
82 chromium)-based MOFs through covalent and coordination
83 bonds, respectively. The performances for H_2 evolution in
84 terms of turnover numbers were improved after inclusion of the
85 catalyst moiety in the MOF, mainly due to its stabilization
86 inside the framework. However, in view of a further
87 optimization of these hybrid catalysts, it should be considered
88 that the introduction of anchoring functions in the trapped
89 catalyst perturbs its first coordination sphere and, consequently,
90 its solution properties are not fully transferred to the molecular
91 material. This issue may be circumvented by direct
92 encapsulation of the unmodified guest into the MOF's pores
93 from solution.[37] Surprisingly, only a few examples of direct
94 encapsulation of organometallic complexes inside MOFs have
95 been reported to date,[38−40] and none are relevant to the
96 domain of catalytic H_2 production. However, this strategy offers
97 two attractive benefits with respect to the covalent attachment
98 method: (i) the applicability to a larger range of functional
99 guests, i.e. all those fitting within the dimensions of the MOF's
100 cavities, and (ii) the higher conformational freedom expected
101 for an encapsulated catalyst.

102 Herein, we report on the first example of incorporation of a
103 [NiFe] hydrogenase mimic into a MOF via the encapsulation
104 strategy. We succeeded in inserting the recently reported
105 $[L^{N2S2}Ni^{II}Fe^{II}Cp(CO)]BF_4$ (**NiFe**; Figure 1) molecular electro-
106 catalyst for proton reduction[41] in the mesoporous Zr-based
107 MOF PCN-777.[37] The resulting **NiFe**@PCN-777 hybrid
108 material was fully characterized in its bulk form and processed
109 in the form of a thin film. In this proof of concept study, we
110 showed that **NiFe**@PCN-777 films retained the electrocatalytic
111 properties of **NiFe** for H^+ reduction on the cyclic voltammetry
112 time scale.

2. RESULTS AND DISCUSSION

113 **2.1. Hybrid NiFe@PCN-777 Material: The Bulk Com-**
114 **pound.** *2.1.1. Choice of the Host System and Encapsulation*
115 *of a [NiFe]-H$_2$ase Mimic.* Heterogenization of a homogeneous
116 organometallic catalyst by encapsulation in the cavities of a
117 MOF requires an estimation of its shape and size and the
118 selection of a MOF with the appropriate pore dimensionality.
119 In this specific case, the catalyst is the metal complex
120 $[L^{N2S2}Ni^{II}Fe^{II}Cp(CO)]BF_4$ (**NiFe**, L^{N2S2} = 2,2′-(2,2′-bipyr-
121 idine-6,6′-diyl)bis(1,1′-diphenylethanethiolate, Cp = cyclopen-
122 tadienyl; Figure 1), a [NiFe]-hydrogenase mimic recently
123 reported by some of us as a homogeneous H_2-evolving
124 electrocatalyst in MeCN solution.[41] This complex is relatively
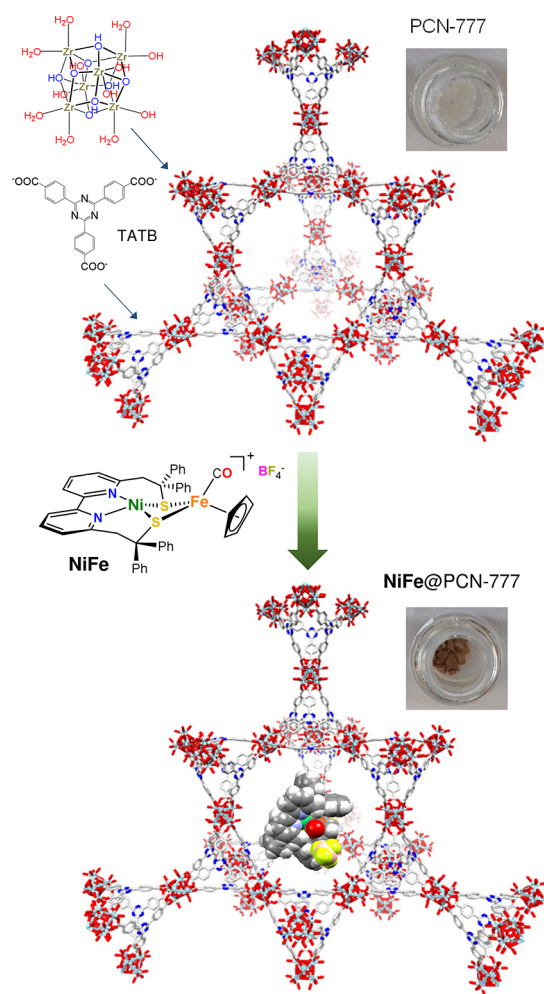125 large (ca. $1.4 \times 0.9 \times 0.8$ nm for the cationic moiety), so that

Figure 1. Encapsulation of $[L^{N2S2}Ni^{II}Fe^{II}Cp(CO)]BF_4$ (**NiFe**) into PCN-777.

only a few MOFs have pores large enough to host it. As a 126
consequence, we selected the mesoporous Zr^{IV}-based MOF 127
PCN-777 as the host system, which exhibits one of the largest 128
cavity sizes among MOFs (i.d. 3.8 nm, with a pore volume 129
distribution centered at 3.4 nm) and that has already been 130
shown to host medium-sized organometallic complexes inside 131
its cavities.[37] PCN-777 features a three-dimensional network 132
generated from the combination of tritopic TATB ligands 133
($TATB^{3−}$ = 4,4′,4″-*s*-triazine-2,4,6-triyl tribenzoate) and 134
octahedral hexanuclear clusters of Zr^{IV}, giving rise to the 135
interconnected void net depicted in Figure 1. PCN-777 offers 136
as additional benefits an excellent chemical stability in the 137
presence of protons, required of a substrate for H_2 evolution, as 138
well as the presence of pendant water and hydroxyl ligands in 139
the Zr coordination sphere, which can act as proton relays to 140
boost catalysis, as previously observed in another Zr^{IV}-MOF 141
(NU-1000).[23] 142

Encapsulation of **NiFe** was achieved by soaking microcrystals 143
of PCN-777 previously activated under high vacuum (5×10^{-5} 144
Torr) at 140 °C into a CH_2Cl_2 solution of the complex. In 145
order to improve the loading capacity, we performed several 146
freeze−pump−thaw cycles on the resulting suspension. 147
Actually, freeze-drying of MOFs is known to increase the 148
permanent porosity of such materials by promoting the 149
sublimation of the included solvent molecules (and thus 150
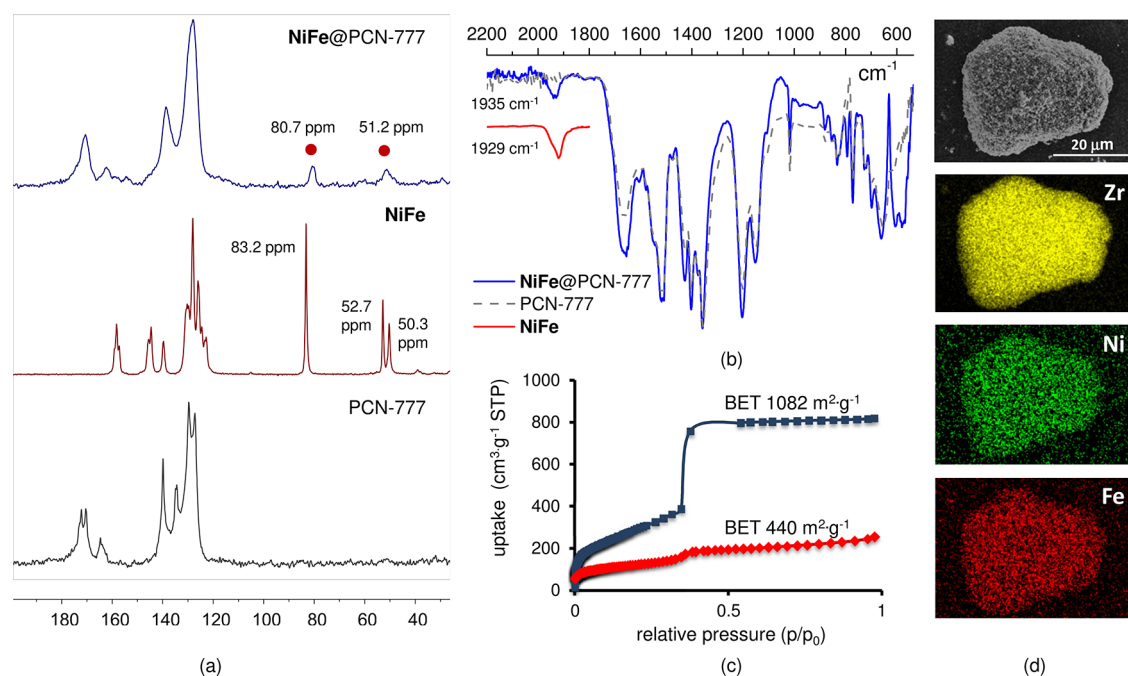circumventing the liquid to gas phase transition and its 151

Figure 2. Characterization of the **NiFe**@PCN-777 bulk material by (a) ^{13}C CP/MAS NMR spectroscopy (the two aliphatic signals attributed to the guest are evidenced by red circles), (b) FTIR spectroscopy, (c) N_2 adsorption isotherms, and (d) SEM micrograph and SEM-EDX elemental maps (points outside the MOF framework correspond to background).

associated capillary forces).[42,43] The **NiFe**@PCN-777 bulk material prepared as described above showed an ~50% increase in the amount of loaded guest with respect to the sample prepared by mere impregnation. A clear indication of the successful incorporation of **NiFe** and of the achievement of a **NiFe**@PCN-777 hybrid material was given by the color change from white to brown observed for the microcrystals of PCN-777 during the synthesis (see Figure 1; the powder of **NiFe** is dark brown).

2.1.2. Physical Characterization. Scanning electron microscopy (SEM, Figure 2d and Figure S2 in the Supporting Information) and powder X-ray diffraction (PXRD, Figure S3 in the Supporting Information) performed on the **NiFe**@PCN-777 bulk material indicated the retention of MOF crystallinity after the incorporation of **NiFe**.

The ^{13}C CP/MAS NMR spectrum confirmed both the incorporation and integrity of **NiFe** (Figure 2a). Indeed, two signals attributed to the guest (CH$_2$ and Cp) are present in the aliphatic region of the spectrum, at roughly the same frequencies (~50 and ~80 ppm, respectively) observed for free **NiFe** complex. These peaks are larger in **NiFe**@PCN-777 than in the crystalline sample of pristine **NiFe**, probably as a consequence of the absence of a preferred orientation of the guests inside the MOF's cavities. The aromatic peaks of the guest are mostly masked by the intense signals of the TATB ligand of PCN-777. The integrity of the incorporated **NiFe** complex was further demonstrated by Fourier transform infrared spectroscopy (FTIR), with a CO stretching vibration band observed at 1935 cm^{-1} (Figure 2b), roughly at the same frequency of free **NiFe** complex (1929 cm^{-1}), while no such absorption was observed for pristine PCN-777.

Measurements of N_2 adsorption isotherms at 77 K (Figure 2c) confirmed the expected decrease in porosity upon inclusion of **NiFe**, with Brunauer–Emmett–Teller (BET) surface areas determined to be 1082[44] and 439 m^2·g^{-1} for activated PCN-777 and **NiFe**@PCN-777, respectively. This decrease in

porosity is consistent with the occupation of a significant portion of the PCN-777 voids by **NiFe**. Coherently, the differential pore volume distribution plot shows a marked decrease in the fraction of pores with a diameter of 3.4 nm (Figure S1 in the Supporting Information).

The SEM-EDX mapping analysis of Ni, Fe, and Zr performed on an extended area of a solid sample of **NiFe**@PCN-777 (Figure 2d) attested to the homogeneous distribution of **NiFe** inside the PCN-777 material. The quantification of the loaded **NiFe** was determined by combining data obtained by inductively coupled plasma-optical emission spectroscopy (ICP-OES) and by energy-dispersed X-ray spectroscopy (EDX). The ratio between S and Ni is approximately 1.9, again pointing to the integrity of the guest into the MOF cavities (a S:Ni ratio of 2 is expected for **NiFe**). The Zr:Ni ratio in the hybrid material was determined to be 10:1 (mol/mol) via both ICP-OES and EDX, which leads to the following overall formula: $Zr_6(O)_4(OH)_{10}(H_2O)_6(TATB)_2 \cdot 0.6[L^{N2S2}Ni^{II}Fe^{II}Cp$-$(CO)]BF_4$. This formula implies 30% of loaded **NiFe**, when it is referenced to the total amount of MOF linker (TATB; this is the usual custom to report loading of covalently bound guests in MOFs).

2.1.3. Host–Guest Interactions and Leaching Tests. Differential scanning calorimetry (DSC) demonstrated the thermal stabilization of **NiFe** inside the MOF's cavities. Indeed, the endothermic decomposition observed at 243 °C for the pure guest was no longer detected in the hybrid material (Figure S4 in the Supporting Information). This is indirect evidence of significant interactions between the guest and the host material, which are also suggested by the slight variations observed in the spectroscopic features of **NiFe** after encapsulation (see Figure 2a,b). To gain further insights into the nature and strength of these interactions, we first compared the efficiency of loading for **NiFe** with that of its neutral precursor complex [L^{N2S2}Ni^{II}] (**Ni**; Scheme S1 in the Supporting Information) to evaluate the possible electrostatic
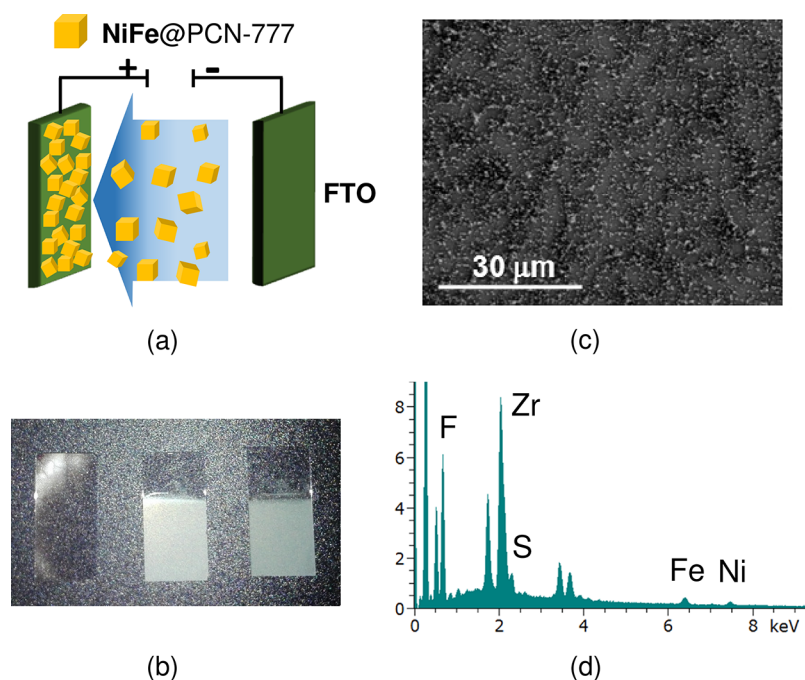
Figure 3. (a) Schematic representation of the EPD process for fabrication of **NiFe**@PCN-777 films. (b) View of FTO-coated glass electrodes (from left to right: bare FTO and FTO coated with free PCN-777 and **NiFe**@PCN-777, respectively). Characterization of the **NiFe**@PCN-777 films by (c) SEM (top-down view) and (d) SEM-EDX.

character of the host−guest interaction. Second, we performed leaching tests from **NiFe**@PCN-777 under different conditions to estimate the strength of the linkage.

Loading of **Ni** into PCN-777 resulted in a material (shown in Figure S5 in the Supporting Information) with a Zr:Ni ratio of 96:1, as determined via ICP-OES. This implies that the amount of guest incorporated is 1 order of magnitude lower than that in the case of **NiFe**, even though **Ni** is smaller than **NiFe** (ca. 1.2 × 0.8 × 0.7 nm). This evidences how the cationic nature of **NiFe** promotes its encapsulation (Figure S6 in the Supporting Information).[45,46]

The host−guest interaction in **NiFe**@PCN-777 is relatively strong. Indeed, only a marginal leaching (<3%) was observed after soaking the hybrid material in CH_2Cl_2 or MeCN for 2 h, as attested by ICP-OES analysis conducted on the filtered solutions (Table S1 in the Supporting Information). However, when a tetrabutylammonium salt such as Bu_4NClO_4 and/or a proton source such as Et_3NHBF_4 are added to an MeCN suspension of **NiFe**@PCN-777, the complex progressively leaches (for example, 25% of the complex was leached after 2 h in the presence of 20 mM of Bu_4NClO_4 and 5 mM of Et_3NHBF_4). This phenomenon can nevertheless be controlled by decreasing either soaking times and/or salt concentrations (for example, only 10% of the complex was leached after 30 min in the presence of 10 mM of Bu_4NClO_4 and 1 mM of Et_3NHBF_4). Leaching of the complex in the presence of ammonium salts can be explained by cationic exchange processes between $[L^{N2S2}Ni^{II}Fe^{II}Cp(CO)]^+$ and the Bu_4N^+/Et_3NH^+ competitor in the MOF's cavities.

Taken together, these data suggest that the **NiFe** inclusion is promoted by electrostatic interactions of the Zr-cluster surface with the $[L^{N2S2}Ni^{II}Fe^{II}Cp(CO)]^+$ cation and/or the BF_4^- anion, even if these interactions are nonspecific (i.e., not dependent on the nature of the ionic couple).

2.2. FTO-Supported Thin Films of NiFe@PCN-777.

2.2.1. Film Processing by Electrophoretic Deposition and Morphological Characterization.

In the attempt to develop an electrocatalytic system for H_2 production based on **NiFe**@PCN-777, we employed electrophoretic deposition (EPD) to deposit a thin film of the hybrid material on a conductive surface. This technique exploits the property of MOF particles to display net negative charges as a consequence of surface defects resulting from missing metal nodes.[47,48] The application of a dc electric field to a suspension of MOF particles in a nonpolar solvent thus results in particle transport and deposition onto a positively polarized fluorine-doped tin oxide (FTO) electrode (Figure 3a), as previously shown by Hupp et al.[49,50] In comparison to the classical epitaxial growth of MOF films under solvothermal conditions (bottom-up approach)[51,52] that requires a long preparation time and postsynthetic modification on the film, EPD has the advantage to be a top-down and one-step method, allowing deposition of a presynthesized and precharacterized bulk MOF material without altering its particle properties. Two identical FTO electrodes were immersed in a colloidal suspension of either **NiFe**@PCN-777 or free PCN-777 (control experiment) in toluene, 0.7 cm apart from one another (Figure S6 in the Supporting Information). Then a constant voltage (120 V) was applied for 5 min between the two electrodes. After the same process was repeated six times, a homogeneous film was formed on the positive electrode (Figure 3b).[53,54]

The morphology of the FTO-supported **NiFe**@PCN-777 films was evaluated by SEM. Top-down micrographs of a representative sample are illustrated in Figure 3c and Figure S8 in the Supporting Information. The images reveal a relatively homogeneous coverage with some degree of aggregation and a surface coverage estimated to ca. 32% (Figure S8), which is comparable to that reported for an [FeFe]-MOF film (33%).[55] The nearly identical morphology and particle size in

comparison to those of the bulk **NiFe**@PCN-777 compound attested to the retention of its structural integrity. These morphological properties are highly reproducible between different samples. EDX spectroscopy (Figure 3d) and ICP-OES analysis (performed on a representative film after digestion in concentrated HNO_3) confirmed the 10:1 Zr:Ni ratio observed in the bulk hybrid material, thus indicating the absence of leaching during the EPD process. The approximate content of **NiFe** in **NiFe**@PCN-777 films was also determined by ICP-OES: taking into account the geometric surface area of the electrode (2.8 cm^2), the average surface concentration of catalyst was found to be 2.6×10^{-9} mol cm^{-2} (see the Supporting Information), corresponding to the equivalent of 20 monolayers of **NiFe** molecules (each **NiFe** molecule having a projected area of 1.3×10^{-14} cm^2; a monolayer corresponds to a surface concentration of 1.3×10^{-10} mol cm^{-2}). Incorporation of **NiFe** into the mesoporous three-dimensional structure of PCN-777 therefore led to a significant increase in the catalyst loading, which is in the same range as for molecular H_2-evolving catalysts immobilized on multiwalled carbon nanotubes (MWCNTs).[16]

2.2.2. Electrochemical Characterization and Electrocatalytic Studies for Proton Reduction. The electrochemical properties of the **NiFe**@PCN-777 films were investigated by cyclic voltammetry (CV, Figure 4a) and compared to those of the homogeneous **NiFe** complex.[41] The CV of **NiFe**@PCN-777 recorded in MeCN/0.02 M Bu$_4$NClO$_4$ displays a reduction wave at $E_{p,c} = -1.37$ V versus Fc$^+$/Fc and one much more intense wave at -2.10 V with a shoulder at $\sim$$-1.90$ V. The peak at -1.37 V corresponds to the reduction of Ni^{II} to Ni^I in the guest molecule, and it is found approximately at the same potential for the homogeneous **NiFe** system ($E_{1/2} = -1.29$ V; see Figure 4a). The main difference is that the reversibility of the signal was lost in the heterogeneous system. In fact, the anodic peak at $\sim$$-1.35$ V found in the complete CV is not related to the cathodic wave at -1.37 V (as shown by comparison with the inset of Figure 4a). This indicates that a chemical reaction follows the electron transfer process, which was confirmed by the loss of intensity of the Ni^{II}/Ni^I redox system from the first to the second scan. Mechanical detachment of the film from FTO can be excluded, as a signal stabilization was observed in the following CV scans. An analogous evolution of the CV was previously observed for the free **NiFe** complex in wet MeCN[41] and was attributed to the coordination of water to the Ni^I center. As mentioned before, water molecules are abundant in the PCN-777 cavities, thus supporting this hypothesis. The second reduction system of **NiFe** (corresponding to the one-electron reduction of the bipyridine scaffold) may correspond to the shoulder at $\sim$$-1.90$ V. It is substantially masked by a wave specific to the host, peaking at -2.10 V in the hybrid material and measured at -2.03 V for pristine PCN-777 coated on FTO. This redox process was assigned to the reduction of water molecules trapped in the PCN-777 pores. Indeed, the signal intensity significantly decreases after drying the PCN-777-coated FTO glass at 140 °C under high vacuum (activation conditions).

Integration of the one-electron reduction peak at $E_{p,c} = -1.37$ V or coulometry during controlled-potential electrolysis (CPE) at -1.4 V allowed an average surface concentration of electroactive **NiFe** catalyst (Γ) inside the PCN-777 MOF of 9.6×10^{-10} mol cm^{-2} to be estimated (see the Supporting Information). On the basis of the total surface concentration of catalyst (see above), this implies that 37% of the **NiFe** units
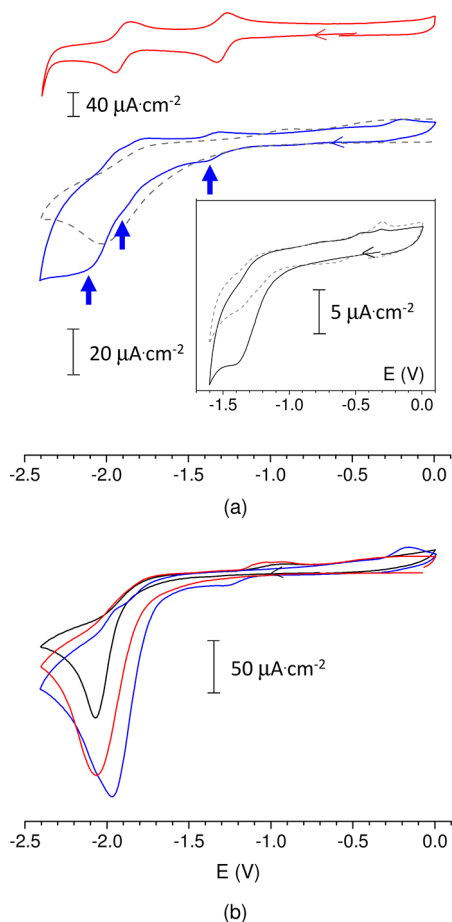

Figure 4. (a) CV of a NiFe@PCN-777 film on FTO (blue −), compared to those of a PCN-777 film (black −) and free **NiFe** (red −, 0.2 mM solution) in MeCN/0.02 M Bu$_4$NClO$_4$. The inset displays the first (−) and second (- - -) scans for the **NiFe**@PCN-777 film (first reduction system). (b) CVs of 1 mM Et$_3$NHBF$_4$ solution in 0.02 M Bu$_4$NClO$_4$/MeCN, in which the working electrode is bare FTO (black −), PCN-777-modified FTO (red −) or **NiFe**@PCN-777-modified FTO (blue −). The scan rate was 50 mV s^{-1}, and potentials are referenced to Fc$^+$/Fc.

encapsulated in PCN-777 are electrochemically addressable. This fraction of electrochemically active complexes inside the PCN-777 film is surprisingly high when the intrinsic insulating character of MOFs is taken into account and when this fraction is compared to that in previously reported MOF (or COF) thin films, which typically exhibit a maximum 10% amount of electroactive centers.[56−58] Systems based on redox-active frameworks such as Fe porphyrins based MOFs represent an exception (77% of electroactive centers).[50] The high electroactivity of the **NiFe**@PCN-777 film is in agreement with the high current density of the CV signal, in comparison for example to the poorly detectable signals from reported MOF films incorporating [FeFe]-hydrogenase mimics.[55,59]

We conclude that the observed current arises not only from the **NiFe** complexes residing at the interface between the electrode surface and the MOF particles but also from a considerable fraction of complexes trapped inside the MOF pores. This is likely a consequence of the high occupancy of the MOF pores (see Figure S1 in the Supporting Information) by the electroactive **NiFe** complex that favors an efficient redox hopping charge-transfer mechanism.[60] The extra-large pore size

in PCN-777 probably facilitates the diffusion of anions out of the MOF, which is required to maintain electroneutrality.[61]

Addition of Et_3NHBF_4 (1 or 5 mM, pK_a = 18.6 in MeCN) as a proton source[62] triggers a catalytic process at $E_{cat} \approx -1.90$ V (Figure 4b and Figure S9 in the Supporting Information), i.e. on the top of the second reduction system of **NiFe**, similarly to the homogeneous system.[41] The current enhancement is associated with the presence of **NiFe** in the PCN-777 cavities, as evidenced from comparison of the H^+ reduction peak measured for **NiFe**@PCN-777-modified FTO with bare FTO or free PCN-777-modified FTO. Controlled-potential electrolysis (CPE) experiments performed at -1.85 V for 2 h in the presence of 5 mM Et_3NHBF_4 confirmed the electrochemical production of H_2 (1.7×10^{-5} mol, corresponding to ∼2400 turnovers vs total **NiFe** catalyst in the case of inactive PCN-777 and FTO) with Faradaic yields of ∼70% (see Figure S10 in the Supporting Information). Unfortunately, no significant differences in current densities and in H_2 production were found in favor of **NiFe**@PCN-777 vs free PCN-777 (both supported on FTO) or bare FTO. This can be tentatively rationalized by (i) the intrinsic electroactivity of FTO for H^+ reduction at low potentials and (ii) the presence of water molecules in the cavities of both MOF materials, acting as proton relays and efficiently promoting direct H_2 evolution even in the absence of **NiFe**. However, an insignificant fraction (less than 5%) of the **NiFe** complex or of its Ni-containing evolution products formed during catalysis were leached after 2 h electrolysis, as attested to by ICP-OES measurements (see the Supporting Information).

3. CONCLUSION

The inclusion of functional molecular components into the cavities of a MOF is an area of active research, as it can lead to the formation of a hybrid material with enhanced properties with respect to the separated systems. Herein, we have reported on the incorporation of a structural and functional model complex of [NiFe]-hydrogenase, namely the H_2-evolution catalyst $[L^{N2S2}Ni^{II}Fe^{II}Cp(CO)]BF_4$ (**NiFe**),[41] into the Zr-based porous coordination network PCN-777 to form an unprecedented [NiFe]-hydrogenase mimicking material.[3] We trapped the cationic complex into the MOF cavities by direct encapsulation through noncovalent host−guest interactions, for which only a few precedents have been reported.[38−40] This method allowed us to achieve similar catalyst loading (∼30%, based on the **NiFe**:MOF linker ratio) in comparison to covalently attached [FeFe]-hydrogenase mimics (∼14−35% range),[21,22,26,27] without requiring derivatization to introduce anchoring functions. Our investigation reveals that direct encapsulation is potentially exploitable for ionic complexes as guests, but with more difficulties for neutral complexes.

The **NiFe**@PCN-777 material, processed in the form of a thin film on a conductive glass substrate, is one of the very few examples of reported electrocatalytic systems based on MOF-type materials for the activation of small molecules[23,50,56,57,63] (even if this material displays an electrocatalytic effect only on the CV time scale). The paucity of MOF-based electrocatalysts is likely due to the inherent poor conductivity of MOFs.[64,65] In the **NiFe**@PCN-777 film, we found a surprisingly high average surface concentration of electroactive **NiFe** catalyst (corresponding to 37% of the total amount of **NiFe** within the MOF), indicating an efficient redox-hopping charge-transfer pathway between **NiFe** units inside the framework and likely responsible for the electrocatalytic capabilities of the hybrid material for proton reduction.

Heterogenization of homogeneous H_2-evolving catalysts by simple encapsulation inside MOF frameworks therefore opens new avenues for the development of new bioinspired electrocatalytic materials. Current efforts by our groups focus on tuning the **NiFe** catalyst to promote catalysis at more positive potential (which will facilitate the achievement of an H_2-evolving electrocatalyst on the CPE time scale) as well as on circumventing guest leaching by tuning pore dimensionality in the host network and optimizing host−guest fitting.

■ ASSOCIATED CONTENT

ⓢ Supporting Information

The Supporting Information is available free of charge on the ACS Publications website at DOI: 10.1021/acs.inorg-chem.7b01824.

> Experimental section, surface concentration calculations, digestion conditions for samples analyzed by ICP-OES, leaching experiments, differential pore volume distribution, PXRD and DSC analyses, SEM images, cyclic voltammetry, and CPE experiments (PDF)

■ AUTHOR INFORMATION

Corresponding Authors
*E-mail for P.P.: paolo.pelagatti@unipr.it.
*E-mail for L.M.: luciano.marchio@unipr.it.
*E-mail for M.G.: marcello.gennari@univ-grenoble-alpes.fr.

ORCID ⃝
Davide Balestri: 0000-0003-3493-9115
Laurent Heux: 0000-0002-1934-4263
Vincent Artero: 0000-0002-6148-8471
Paolo Pelagatti: 0000-0002-6926-2928
Luciano Marchio: 0000-0002-0025-1104
Marcello Gennari: 0000-0001-5205-1123

Notes
The authors declare no competing financial interest.

■ REFERENCES

(1) Nocera, D. G. The Artificial Leaf. *Acc. Chem. Res.* **2012**, *45*, 767−776.

(2) Cook, T. R.; Dogutan, D. K.; Reece, S. Y.; Surendranath, Y.; Teets, T. S.; Nocera, D. G. Solar Energy Supply and Storage for the Legacy and Nonlegacy Worlds. *Chem. Rev.* **2010**, *110*, 6474−6502.

(3) McKone, J. R.; Marinescu, S. C.; Brunschwig, B. S.; Winkler, J. R.; Gray, H. B. Earth-abundant hydrogen evolution electrocatalysts. *Chem. Sci.* **2014**, *5*, 865−878.

(4) Dempsey, J. L.; Winkler, J. R.; Gray, H. B. In *Comprehensive Inorganic Chemistry II*, 2nd ed.; Poeppelmeier, K., Ed.; Elsevier: Amsterdam, 2013; pp 553−565.

(5) Lubitz, W.; Ogata, H.; Rüdiger, O.; Reijerse, E. Hydrogenases. *Chem. Rev.* **2014**, *114*, 4081−4148.

(6) Vignais, P. M.; Billoud, B. Occurrence, classification, and biological function of hydrogenases: An overview. *Chem. Rev.* **2007**, *107*, 4206−4272.

(7) Simmons, T. R.; Berggren, G.; Bacchi, M.; Fontecave, M.; Artero, V. Mimicking hydrogenases: From biomimetics to artificial enzymes. *Coord. Chem. Rev.* **2014**, *270−271*, 127−150.

(8) Schilter, D.; Camara, J. M.; Huynh, M. T.; Hammes-Schiffer, S.; Rauchfuss, T. B. Hydrogenase Enzymes and Their Synthetic Models: The Role of Metal Hydrides. *Chem. Rev.* **2016**, *116*, 8693−8749.

(9) Rauchfuss, T. B. Diiron Azadithiolates as Models for the [FeFe]-Hydrogenase Active Site and Paradigm for the Role of the Second Coordination Sphere. *Acc. Chem. Res.* **2015**, *48*, 2107−2116.

(10) Kaur-Ghumaan, S.; Stein, M. [NiFe] hydrogenases: how close do structural and functional mimics approach the active site? *Dalton Trans.* **2014**, *43*, 9392−9405.

(11) Caserta, G.; Roy, S.; Atta, M.; Artero, V.; Fontecave, M. Artificial hydrogenases: biohybrid and supramolecular systems for catalytic hydrogen production or uptake. *Curr. Opin. Chem. Biol.* **2015**, *25*, 36−47.

(12) Nath, I.; Chakraborty, J.; Verpoort, F. Metal organic frameworks mimicking natural enzymes: a structural and functional analogy. *Chem. Soc. Rev.* **2016**, *45*, 4127−4170.

(13) Zhang, M.; Gu, Z.-Y.; Bosch, M.; Perry, Z.; Zhou, H.-C. Biomimicry in metal−organic materials. *Coord. Chem. Rev.* **2015**, *293−294*, 327−356.

(14) Meyer, K.; Ranocchiari, M.; van Bokhoven, J. A. Metal organic frameworks for photo-catalytic water splitting. *Energy Environ. Sci.* **2015**, *8*, 1923−1937.

(15) Pullen, S.; Ott, S. Photochemical Hydrogen Production with Metal−Organic Frameworks. *Top. Catal.* **2016**, *59*, 1712−1721.

(16) Coutard, N.; Kaeffer, N.; Artero, V. Molecular engineered nanomaterials for catalytic hydrogen evolution and oxidation. *Chem. Commun.* **2016**, *52*, 13728−13748.

(17) Peters, A. W.; Li, Z.; Farha, O. K.; Hupp, J. T. Toward Inexpensive Photocatalytic Hydrogen Evolution: A Nickel Sulfide Catalyst Supported on a High-Stability Metal−Organic Framework. *ACS Appl. Mater. Interfaces* **2016**, *8*, 20675−20681.

(18) Kim, D.; Whang, D. R.; Park, S. Y. Self-Healing of Molecular Catalyst and Photosensitizer on Metal−Organic Framework: Robust Molecular System for Photocatalytic H2 Evolution from Water. *J. Am. Chem. Soc.* **2016**, *138*, 8698−8701.

(19) Dai, X.; Liu, M.; Li, Z.; Jin, A.; Ma, Y.; Huang, X.; Sun, H.; Wang, H.; Zhang, X. Molybdenum Polysulfide Anchored on Porous Zr-Metal Organic Framework To Enhance the Performance of Hydrogen Evolution Reaction. *J. Phys. Chem. C* **2016**, *120*, 12539−12548.

(20) Hou, C.-C.; Li, T.-T.; Cao, S.; Chen, Y.; Fu, W.-F. Incorporation of a [Ru(dcbpy)(bpy)2]2+ photosensitizer and a Pt(dcbpy)Cl2 catalyst into metal-organic frameworks for photocatalytic hydrogen evolution from aqueous solution. *J. Mater. Chem. A* **2015**, *3*, 10386−10394.

(21) Sasan, K.; Lin, Q.; Mao, C.; Feng, P. Incorporation of iron hydrogenase active sites into a highly stable metal-organic framework for photocatalytic hydrogen generation. *Chem. Commun.* **2014**, *50*, 10390−10393.

(22) Pullen, S.; Fei, H.; Orthaber, A.; Cohen, S. M.; Ott, S. Enhanced Photochemical Hydrogen Production by a Molecular Diiron Catalyst Incorporated into a Metal−Organic Framework. *J. Am. Chem. Soc.* **2013**, *135*, 16997−17003.

(23) Hod, I.; Deria, P.; Bury, W.; Mondloch, J. E.; Kung, C.-W.; So, M.; Sampson, M. D.; Peters, A. W.; Kubiak, C. P.; Farha, O. K.; Hupp, J. T. A porous proton-relaying metal-organic framework material that accelerates electrochemical hydrogen evolution. *Nat. Commun.* **2015**, *6*, 8304.

(24) Downes, C. A.; Marinescu, S. C. Efficient Electrochemical and Photoelectrochemical H2 Production from Water by a Cobalt Dithiolene One-Dimensional Metal-Organic Surface. *J. Am. Chem. Soc.* **2015**, *137*, 13740−13743.

(25) Clough, A. J.; Yoo, J. W.; Mecklenburg, M. H.; Marinescu, S. C. Two-Dimensional Metal-Organic Surfaces for Efficient Hydrogen Evolution from Water. *J. Am. Chem. Soc.* **2015**, *137*, 118−121.

(26) Roy, S.; Pascanu, V.; Pullen, S.; Gonzalez Miera, G.; Martín-Matute, B.; Ott, S. Catalyst accessibility to chemical reductants in metal-organic frameworks. *Chem. Commun.* **2017**, *53*, 3257−3260.

(27) Fei, H.; Pullen, S.; Wagner, A.; Ott, S.; Cohen, S. M. Functionalization of robust Zr(iv)-based metal-organic framework films via a postsynthetic ligand exchange. *Chem. Commun.* **2015**, *51*, 66−69.

(28) Janiak, C.; Vieth, J. K. MOFs, MILs and more: concepts, properties and applications for porous coordination networks (PCNs). *New J. Chem.* **2010**, *34*, 2366−2388.

(29) Furukawa, H.; Cordova, K. E.; O'Keeffe, M.; Yaghi, O. M. The Chemistry and Applications of Metal-Organic Frameworks. *Science* **2013**, *341*, 974.

(30) Kim, C. R.; Uemura, T.; Kitagawa, S. Inorganic nanoparticles in porous coordination polymers. *Chem. Soc. Rev.* **2016**, *45*, 3828−3845.

(31) Jiang, J.; Zhao, Y.; Yaghi, O. M. Covalent Chemistry beyond Molecules. *J. Am. Chem. Soc.* **2016**, *138*, 3255−3265.

(32) Wang, C.; Liu, D.; Lin, W. Metal-Organic Frameworks as A Tunable Platform for Designing Functional Molecular Materials. *J. Am. Chem. Soc.* **2013**, *135*, 13222−13234.

(33) Gascon, J.; Corma, A.; Kapteijn, F.; Llabres i Xamena, F. X. Metal Organic Framework Catalysis: Quo vadis? *ACS Catal.* **2014**, *4*, 361−378.

(34) Gutzler, R.; Stepanow, S.; Grumelli, D.; Lingenfelder, M.; Kern, K. Mimicking Enzymatic Active Sites on Surfaces for Energy Conversion Chemistry. *Acc. Chem. Res.* **2015**, *48*, 2132−2139.

(35) Cohen, S. M.; Zhang, Z.; Boissonnault, J. A. Toward "metalloMOFzymes": Metal−Organic Frameworks with Single-Site Metal Catalysts for Small-Molecule Transformations. *Inorg. Chem.* **2016**, *55*, 7281−7290.

(36) Pullen, S.; Roy, S.; Ott, S. [FeFe] Hydrogenase active site model chemistry in a UiO-66 metal-organic framework. *Chem. Commun.* **2017**, *53*, 5227−5230.

(37) Feng, D.; Wang, K.; Su, J.; Liu, T.-F.; Park, J.; Wei, Z.; Bosch, M.; Yakovenko, A.; Zou, X.; Zhou, H.-C. A Highly Stable Zeotype Mesoporous Zirconium Metal-Organic Framework with Ultralarge Pores. *Angew. Chem., Int. Ed.* **2015**, *54*, 149−154.

(38) Grigoropoulos, A.; Whitehead, G. F. S.; Perret, N.; Katsoulidis, A. P.; Chadwick, F. M.; Davies, R. P.; Haynes, A.; Brammer, L.; Weller, A. S.; Xiao, J.; Rosseinsky, M. J. Encapsulation of an organometallic cationic catalyst by direct exchange into an anionic MOF. *Chem. Sci.* **2016**, *7*, 2037−2050.

(39) Chołuj, A.; Zieliński, A.; Grela, K.; Chmielewski, M. J. Metathesis@MOF: Simple and Robust Immobilization of Olefin Metathesis Catalysts inside (Al)MIL-101-NH2. *ACS Catal.* **2016**, *6*, 6343−6349.

(40) Spekreijse, J.; Öhrström, L.; Sanders, J. P. M.; Bitter, J. H.; Scott, E. L. Mechanochemical Immobilisation of Metathesis Catalysts in a Metal−Organic Framework. *Chem. - Eur. J.* **2016**, *22*, 15437−15443.

(41) Brazzolotto, D.; Gennari, M.; Queyriaux, N.; Simmons, T. R.; Pecaut, J.; Demeshko, S.; Meyer, F.; Orio, M.; Artero, V.; Duboc, C. Nickel-centred proton reduction catalysis in a model of [NiFe] hydrogenase. *Nat. Chem.* **2016**, *8*, 1054−1060.

(42) Ma, L.; Jin, A.; Xie, Z.; Lin, W. Freeze Drying Significantly Increases Permanent Porosity and Hydrogen Uptake in 4,4-Connected

G

Metal−Organic Frameworks. *Angew. Chem., Int. Ed.* **2009**, *48*, 9905−9908.

(43) Mondloch, J. E.; Karagiaridi, O.; Farha, O. K.; Hupp, J. T. Activation of metal-organic framework materials. *CrystEngComm* **2013**, *15*, 9258−9264.

(44) The discrepancy with the previously reported value of BET surface area for PCN-777 (2008 m$^{2.}$ g^{-1}, see ref 37) can be attributed to a lower crystallinity of the sample used in the present study, probably due to different activation conditions.

(45) Peng, Y.; Huang, H.; Liu, D.; Zhong, C. Radioactive Barium Ion Trap Based on Metal−Organic Framework for Efficient and Irreversible Removal of Barium from Nuclear Wastewater. *ACS Appl. Mater. Interfaces* **2016**, *8*, 8527−8535.

(46) Gao, L.; Li, C.-Y. V.; Chan, K.-Y.; Chen, Z.-N. Metal−Organic Framework Threaded with Aminated Polymer Formed in Situ for Fast and Reversible Ion Exchange. *J. Am. Chem. Soc.* **2014**, *136*, 7209−7212.

(47) Gutov, O. V.; Hevia, M. G.; Escudero-Adán, E. C.; Shafir, A. Metal−Organic Framework (MOF) Defects under Control: Insights into the Missing Linker Sites and Their Implication in the Reactivity of Zirconium-Based Frameworks. *Inorg. Chem.* **2015**, *54*, 8396−8400.

(48) Shearer, G. C.; Chavan, S.; Bordiga, S.; Svelle, S.; Olsbye, U.; Lillerud, K. P. Defect Engineering: Tuning the Porosity and Composition of the Metal−Organic Framework UiO-66 via Modulated Synthesis. *Chem. Mater.* **2016**, *28*, 3749−3761.

(49) Hod, I.; Bury, W.; Karlin, D. M.; Deria, P.; Kung, C.-W.; Katz, M. J.; So, M.; Klahr, B.; Jin, D.; Chung, Y.-W.; Odom, T. W.; Farha, O. K.; Hupp, J. T. Directed growth of electroactive metal-organic framework thin films using electrophoretic deposition. *Adv. Mater.* **2014**, *26*, 6295−6300.

(50) Hod, I.; Sampson, M. D.; Deria, P.; Kubiak, C. P.; Farha, O. K.; Hupp, J. T. Fe-Porphyrin-Based Metal-Organic Framework Films as High-Surface Concentration, Heterogeneous Catalysts for Electrochemical Reduction of CO2. *ACS Catal.* **2015**, *5*, 6302−6309.

(51) Betard, A.; Fischer, R. A. Metal-Organic Framework Thin Films: From Fundamentals to Applications. *Chem. Rev.* **2012**, *112*, 1055−1083.

(52) Zhuang, J.-L.; Terfort, A.; Wöll, C. Formation of oriented and patterned films of metal−organic frameworks by liquid phase epitaxy: A review. *Coord. Chem. Rev.* **2016**, *307*, 391−424.

(53) When toluene is replaced by other solvents (CH$_2$Cl$_2$, DMF) or solvent mixtures (DMF−toluene), no film formation or much thinner and poorly homogeneous films were observed.

(54) When the deposit is formed from pristine PCN-777 rather than directly from **NiFe@PCN-777**, two further steps are required, the activation of the FTO-MOF film and the successive loading of **NiFe**, which are accompanied by two additional issues: (i) film cracking when activating PCN-777 at 140 °C under vacuum (Figure S7 in the Supporting Information) and (ii) mechanical detachment of the material from FTO when **NiFe** loading was carried out by freeze−pump−thaw.

(55) Mijangos, E.; Roy, S.; Pullen, S.; Lomoth, R.; Ott, S. Evaluation of two- and three-dimensional electrode platforms for the electrochemical characterization of organometallic catalysts incorporated in non-conducting metal-organic frameworks. *Dalton Trans.* **2017**, *46*, 4907−4911.

(56) Johnson, B. A.; Bhunia, A.; Ott, S. Electrocatalytic water oxidation by a molecular catalyst incorporated into a metal-organic framework thin film. *Dalton Trans.* **2017**, *46*, 1382−1388.

(57) Kung, C.-W.; Mondloch, J. E.; Wang, T. C.; Bury, W.; Hoffeditz, W.; Klahr, B. M.; Klet, R. C.; Pellin, M. J.; Farha, O. K.; Hupp, J. T. Metal−Organic Framework Thin Films as Platforms for Atomic Layer Deposition of Cobalt Ions To Enable Electrocatalytic Water Oxidation. *ACS Appl. Mater. Interfaces* **2015**, *7*, 28223−28230.

(58) Lin, S.; Diercks, C. S.; Zhang, Y.-B.; Kornienko, N.; Nichols, E. M.; Zhao, Y.; Paris, A. R.; Kim, D.; Yang, P.; Yaghi, O. M.; Chang, C. J. Covalent organic frameworks comprising cobalt porphyrins for catalytic CO2 reduction in water. *Science* **2015**, *349*, 1208.

(59) Fei, H.; Pullen, S.; Wagner, A.; Ott, S.; Cohen, S. M. Functionalization of robust Zr(IV)-based metal-organic framework films via a postsynthetic ligand exchange. *Chem. Commun.* **2015**, *51*, 66−69.

(60) Ahrenholtz, S. R.; Epley, C. C.; Morris, A. J. Solvothermal Preparation of an Electrocatalytic Metalloporphyrin MOF Thin Film and its Redox Hopping Charge-Transfer Mechanism. *J. Am. Chem. Soc.* **2014**, *136*, 2464−2472.

(61) Hod, I.; Bury, W.; Gardner, D. M.; Deria, P.; Roznyatovskiy, V.; Wasielewski, M. R.; Farha, O. K.; Hupp, J. T. Bias-Switchable Permselectivity and Redox Catalytic Activity of a Ferrocene-Functionalized, Thin-Film Metal-Organic Framework Compound. *J. Phys. Chem. Lett.* **2015**, *6*, 586−591.

(62) Izutsu, K. *Acid-Base Dissociation Constants in Dipolar Aprotic Solvents*; Blackwell Scientific: Oxford, U.K., 1990.

(63) Yang, L.; Kinoshita, S.; Yamada, T.; Kanda, S.; Kitagawa, H.; Tokunaga, M.; Ishimoto, T.; Ogura, T.; Nagumo, R.; Miyamoto, A.; Koyama, M. A metal-organic framework as an electrocatalyst for ethanol oxidation. *Angew. Chem., Int. Ed.* **2010**, *49*, 5348−5351.

(64) Morozan, A.; Jaouen, F. Metal organic frameworks for electrochemical applications. *Energy Environ. Sci.* **2012**, *5*, 9269−9290.

(65) D'Alessandro, D. M. Exploiting redox activity in metal-organic frameworks: concepts, trends and perspectives. *Chem. Commun.* **2016**, *52*, 8957−8971.